JACS
JOURNAL OF THE AMERICAN CHEMICAL SOCIETY
Article
Cite This: J. Am. Chem. Soc. 2019, 141, 20215−20221
pubs.acs.org/JACS

Pyrazine-Flanked Diketopyrrolopyrrole (DPP): A New Polymer Building Block for High-Performance n-Type Organic Thermoelectrics

Xinwen Yan,[†,§,#] Miao Xiong,[‡,§,#] Jia-Tong Li,[†] Song Zhang,[∥] Zachary Ahmad,[∥] Yang Lu,[‡,§] Zi-Yuan Wang,[‡,§] Ze-Fan Yao,[‡,§] Jie-Yu Wang,[‡,§] Xiaodan Gu,[∥] and Ting Lei*[,†,‡,⊥]

[†]Department of Materials Science and Engineering, College of Engineering, Peking University, Beijing 100871, China
[‡]Key Laboratory of Polymer Chemistry and Physics of Ministry of Education, Peking University, Beijing 100871, China
[§]College of Chemistry and Molecular Engineering, Peking University, Beijing 100871, China
[∥]School of Polymer Science and Engineering, The University of Southern Mississippi, Hattiesburg, Mississippi 39406, United States
[⊥]Beijing Key Laboratory for Magnetoelectric Materials and Devices, Peking University, Beijing 100871, China

Supporting Information

ABSTRACT: n-Doped conjugated polymers usually show low electrical conductivities and low thermoelectric power factors, limiting their applications in n-type organic thermoelectrics. Here, we report the synthesis of a new diketopyrrolopyrrole (DPP) derivative, pyrazine-flanked DPP (PzDPP), with the deepest LUMO level in all the reported DPP derivatives. Based on PzDPP, a donor−acceptor copolymer, P(PzDPP-CT2), is synthesized. The polymer displays a deep LUMO energy level and strong interchain interaction with a short $\pi-\pi$ stacking distance of 3.38 Å. When doped with n-dopant *N*-DMBI, P(PzDPP-CT2) exhibits high n-type electrical conductivities of up to 8.4 S cm^{-1} and power factors of up to 57.3 μW m^{-1} K^{-2}. These values are much higher than previously reported n-doped DPP polymers, and the power factor also ranks the highest in solution-processable n-doped conjugated polymers. These results suggest that PzDPP is a promising high-performance building block for n-type organic thermoelectrics and also highlight that, without sacrificing polymer interchain interactions, efficient n-doping can be realized in conjugated polymers with careful molecular engineering.

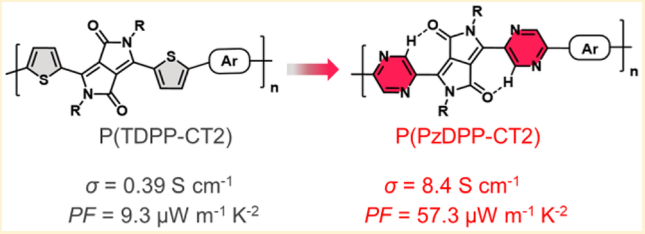

INTRODUCTION

Conjugated polymers are an intriguing class of semiconductors for printed optoelectronics, energy conversion, and storage devices since they are solution-processable and lightweight and can be fabricated into flexible devices.[1−3] Compared with inorganic alloys, organic thermoelectrics (OTEs) have shown great potential as thermoelectric materials due to their low toxicity, low thermal conductivity, and good solution processability. p-Type polymer poly(3,4-ethylenedioxythiophene) (PEDOT) has exhibited a high thermoelectric figure of merit (*ZT*) over 0.4, which is already comparable to that of inorganic materials at low temperature. The good thermoelectric performance and above-mentioned unique properties of polymers make them particularly suitable for applications requiring distributed power generation, such as mobile devices, wearable electronics, and sensor networks.[4]

To achieve highly efficient thermoelectric modules, both p- and n-type conjugated polymers with comparable performance are required. However, the thermoelectric performance of n-doped conjugated polymers is far inferior to their p-type counterparts. The high *ZT* values of PEDOT are mainly ascribed to its high electrical conductivities (>1000 S cm^{-1}) and high power factors (>300 μW m^{-1} K^{-2}).[5] Although high electrical conductivities over 1000 S cm^{-1} have been obtained in p-doped polymers,[6] only a few n-doped polymers are demonstrated to have electrical conductivities approaching or over 1 S cm^{-1} with power factors usually below 10 μW m^{-1} K^{-2}.[7−17]

The past few years have witnessed the rapid improvement of the charge carrier mobilities of donor−acceptor (D−A) conjugated polymers, largely due to the innovation of high-performance polymer building blocks.[18−23] Among them, diketopyrrolopyrrole (DPP) is one of the most extensively studied building blocks.[20] D−A polymers based on DPP have exhibited high hole mobilities over 10 cm^2 V^{-1} s^{-1}[24] and high electron mobilities over 5 cm^2 V^{-1} s^{-1}.[22] However, the electrical conductivities of n-doped DPP polymers are always low (usually 0.1−1 S cm^{-1}), although DPP polymers have shown comparable or even higher charge carrier mobilities (>1 cm^2 V^{-1} s^{-1}) than those of p-type conjugated polymers (e.g., ∼1 cm^2 V^{-1} s^{-1} for PEDOT or PBTTT, etc.).[25] Theoretically,

Received: September 18, 2019
Published: November 27, 2019

DOI: 10.1021/jacs.9b10107
J. Am. Chem. Soc. 2019, 141, 20215−20221

electrical conductivity (σ) is determined by the charge carrier concentration (n) and charge carrier mobility (μ) ($\sigma = n\mu q$; q is the elementary charge). Therefore, the low n-type electrical conductivities of DPP-based polymers are mainly due to their low n-doping levels. Recently, to enhance the n-doping level in DPP polymer, Chabinyc et al. used a twisted nonplanar donor moiety and demonstrated an improved n-doped electrical conductivity of 0.45 S cm^{-1}.[11] Pei et al. used a fluorinated donor moiety to reduce the donor−acceptor character of a DPP-based polymer and achieved currently the highest n-type electrical conductivity (1.3 S cm^{-1}) in n-doped D−A type polymers and a maximum thermoelectric power factor of 4.65 μW m^{-1} K^{-2}.[9] Nevertheless, these values are still much lower than those of p-type materials, and more efforts are needed to further improve the doping efficiency and thermoelectric performance of n-doped conjugated polymers.

Here we report the synthesis of a new DPP derivative, pyrazine-flanked DPP (PzDPP), which has the deepest LUMO energy level in all reported DPP derivatives (Figure 1a). We

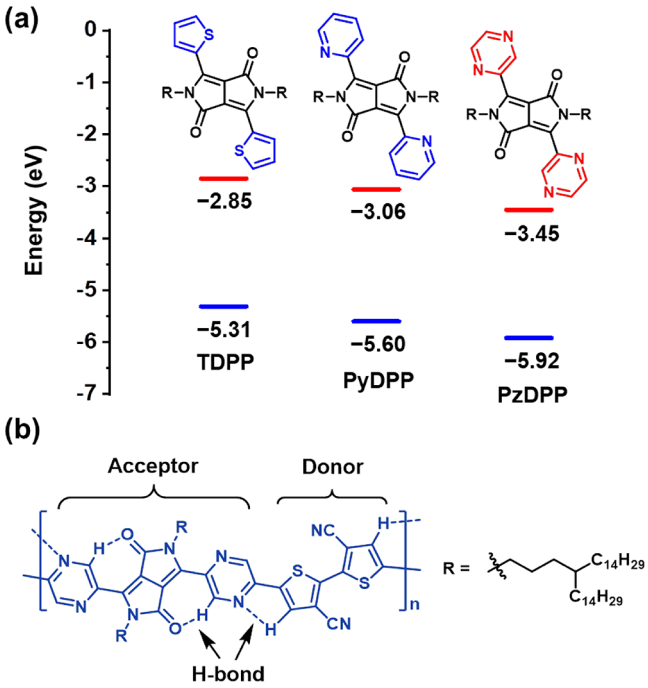

Figure 1. (a) Chemical structures and calculated HOMO/LUMO levels of two most studied DPP building blocks (thiophene-flanked and pyridine-flanked DPP) and PzDPP (R = Me, B3LYP/6-311+G(d,p)). (b) Structure of the D−A polymer P(PzDPP-CT2).

also employed an electron-deficient donor moiety, 3,3′-dicyano-2,2′-bithiophene, to polymerize with PzDPP and obtained a new donor−acceptor polymer, P(PzDPP-CT2) (Figure 1b). The polymer exhibits a planar and conformation-locked backbone structure with a deep LUMO (lowest unoccupied molecular orbital) level down to −4.03 eV. When doped with n-type dopant (4-(1,3-dimethyl-2,3-dihydro-1*H*-benzoimidazol-2-yl)phenyl)dimethylamine (*N*-DMBI) (Scheme 1), P(PzDPP-CT2) displays the highest electrical conductivity of 8.4 S cm^{-1} and power factors of up to 57.3 μW m^{-1} K^{-2}. The conductivity is obviously higher than other n-doped D−A type polymers, and the power factor also ranks the highest in n-type solution-processable polymer thermoelectric materials.[8−10]

RESULTS AND DISCUSSIONS

Polymer Design, Synthesis, and Characterization. Scheme 1 illustrates the synthetic routes to PzDPP and polymer P(PzDPP-CT2). The synthetic procedure of PzDPP is quite different from the commonly used thiophene- or pyridine-flanked DPP unit that can be directly synthesized from 2-thiophenecarbonitrile or 5-bromo-2-pyridinecarbonitrile.[22,26] The bromine atom connected to the pyrazine is highly reactive and easily substituted with the bases in the reaction system, including *tert*-pentoxide or isopropoxide. The high reactivity of the bromine atom is probably due to the strong electron-deficient nature of PzDPP. After alkylation, we isolated a mixture of three compounds: **3a** (X = two *tert*-pentyloxy), **3b** (X = one *tert*-pentyloxy and one isopropoxy), and **3c** (X = two isopropoxy). To obtain the bromo-substituted PzDPP unit for polymerization, the mixture was successively treated with BBr_3 and concentrated HCl to remove the isopropyl and *tert*-pentyl groups, and the resulting crude product was treated with trifluoromethanesulfonic anhydride to afford compound **4**. The trifluoromethanesulfonic group can be readily converted to bromine with the treatment of tetrabutylammonium bromide, which is also ascribed to the strong electron-deficient nature of PzDPP, yielding the PzDPP monomer **5** ready for polymerization.

Recent studies have suggested that electron-deficient modification of the donor moiety can enhance the electron affinity of the D−A polymers, leading to better miscibility with n-dopants and improved n-doping efficiency.[8,9] Thus, 3,3′-dicyano-2,2′-bithiophene was chosen as the donor moiety, due to its good planarity and strong electron-withdrawing property of the two cyano groups. Polymer P(PzDPP-CT2) was synthesized through the Pd-catalyzed Stille coupling reaction between PzDPP and 5,5′-bis(trimethylstannyl)-3,3′-dicyano-2,2′-bithiophene in the presence of a small amount of CuI as the cocatalyst.[27] To understand the important role of the PzDPP, a reference polymer, P(TDPP-CT2), containing the most studied thiophene-flanked DPP (TDPP) building block, was also synthesized. Both polymers were purified by Soxhlet extraction, and their chemical structures were verified by high-temperature ^{1}H NMR spectra (details in the Supporting Information (SI)). Both polymers have similar molecular weights (M_n) around 30 kDa, which were evaluated by high-temperature gel permeation chromatography (GPC) at 150 °C using 1,2,4-tricholorobenzene (TCB) as eluent (Table 1). Both polymers show excellent thermal stability with decomposition temperature over 380 °C and no observable phase transition in the range from room temperature to 300 °C (Figures S1−S3 in the SI).

Both polymers exhibit similar absorption features (Figure S4 in the SI). P(TDPP-CT2) has two absorption peaks at 734 and 797 nm, while P(PzDPP-CT2) has a blue-shifted maximum absorption peak at 713 nm with a shoulder peak at 655 nm in solution. In film, both polymers exhibit slightly red-shifted spectra with increased vibrational peaks, indicating that both polymers may have more planar backbones in the solid state. Temperature-dependent absorption spectra reveal that both polymers showed strong aggregation even in dilute (10^{-5} M) TCB solutions at high temperature, and the PzDPP polymer exhibited stronger aggregation compared to the TDPP polymer (see Figure S5 for detailed discussions). Density functional theory (DFT) calculations show that, similar to the TDPP, PzDPP also has a small dihedral angle between the

DOI: 10.1021/jacs.9b10107
J. Am. Chem. Soc. 2019, 141, 20215−20221

Scheme 1. Synthetic Routes to P(PzDPP-CT2) and the Reference Polymer P(TDPP-CT2)[a]

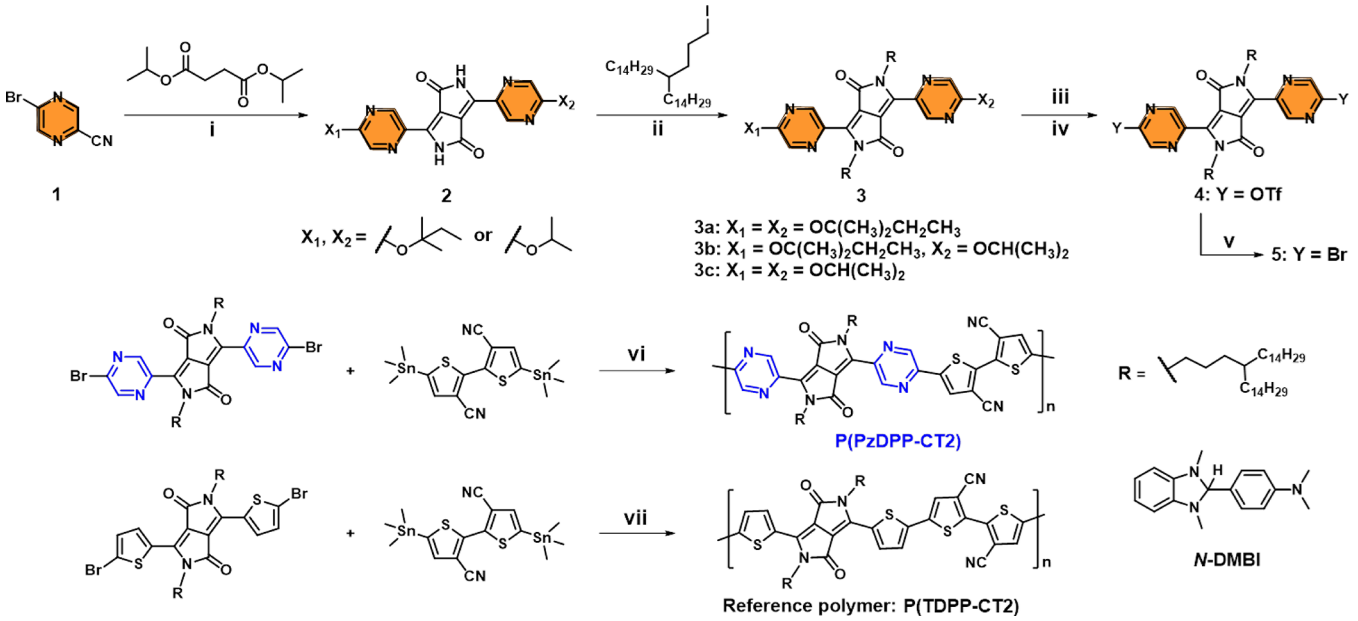

[a]Reagents and conditions: (i) Na, $FeCl_3$, 2-methyl-2-butanol, 85 °C, 12 h. (ii) K_2CO_3, 18-crown-6, DMF, 70 °C, 18 h. (iii) BBr_3, dichloromethane, −78 °C to rt, 2 h; conc HCl, 1,4-dioxane, reflux, 0.5 h. (iv) Tf_2O, pyridine, dichloromethane, rt, 1.5 h. (v) $Bu_4N^+Br^-$, toluene, 85 °C, 12 h. (vi) $Pd_2(dba)_3$, P(*o*-Tol)$_3$, CuI, DMF/toluene, 110 °C. (vii) $Pd_2(dba)_3$, P(*o*-Tol)$_3$, toluene, 110 °C.

Table 1. Summary of the Molecular Weights, Energy Levels, Electron Mobilities, and $\pi-\pi$ Stacking Distances of the Pristine Polymers and Electrical Conductivity Maxima and PF Maxima of the *N*-DMBI-Doped Polymers

polymer	M_n [kDa]	PDI	E_g[a] [eV]	E_{HOMO}[a] [eV]	E_{LUMO}[a] [eV]	μ_e[b] [cm^2 V^{-1} s^{-1}]	σ_{max} [S cm^{-1}]	PF_{max} [μW m^{-1} K^{-2}]	$d_{\pi-\pi}$ [Å]
P(PzDPP-CT2)	28.5	2.90	1.86	−5.89	−4.03	0.79	8.4	57.3	3.38
P(TDPP-CT2)	34.0	2.14	1.91	−5.61	−3.70	0.32	0.39	9.3	3.53

[a]Estimated from the cyclic voltammetry (CV) measurement. [b]Maximal mobilities measured using field-effect transistor with a top-gate bottom-contact configuration.

pyrazine and the DPP core (ϕ_1 = 0.24°) (Figure 2a). Even though the dihedral angle between the two thiophene units slightly rises to 5.58°, the optimized structure of the P(PzDPP-CT2) trimer still exhibits an almost coplanar conformation (Figure S9 in the SI). Calculations also show that the O···H and N···H distances in the polymer are smaller than the sum of the van der Waals radii of O, N, and H (1.52, 1.55, and 1.20 Å, respectively), indicating that the pyrazine moiety can form intramolecular hydrogen bonds along the polymer backbone, leading to a rigid and planar backbone and efficient intrachain charge transport. According to the cyclic voltammetry (CV) measurement (Figure S8 in the SI), the PzDPP monomer shows a deep LUMO level of −3.77 eV, 0.16 eV lower than the pyridine-flanked DPP (PyDPP). This result is consistent with the theoretical calculation. To our knowledge, PzDPP is currently the most electron-deficient DPP building block in the literature.[20] The LUMO and HOMO (highest occupied molecular orbital) energy levels of P(PzDPP-CT2) reach −4.03 and −5.89 eV, respectivel,. 0.33 and 0.28 eV lower than that of P(TDPP-CT2) (−3.70 and −5.61 eV) (Figure 2b). Clearly, P(PzDPP-CT2) shows stronger electron affinity than the reference TDPP polymer.

Characterization of the Doped Polymers. *N*-DMBI was used to dope both polymers due to its strong n-doping ability.[28−30] UV−vis−NIR absorption spectroscopy was used to evaluate the n-doping efficiency for both polymers (Figure 2c, Figures S6 and S7 in the SI). No obvious absorption above 900 nm is observed in their pristine films. After *N*-DMBI doping, both polymers exhibit two typical (bi)polaron absorption bands in the near-infrared region, suggesting that both polymers can be successfully n-doped using *N*-DMBI. For P(PzDPP-CT2), the new absorption bands from 800 to 1300 nm and above 1300 nm can be ascribed to the P2 and P1 absorptions of the (bi)polaron (Figure 2c).[31] The (bi)polaron absorption for n-doped P(TDPP-CT2) can be similarly identified. The main absorption peaks of both doped polymer films undergo a slight blue-shift, which also suggests the formation of (bi)polaronic bands.[31,32] Compared with P(TDPP-CT2), P(PzDPP-CT2) shows much stronger (bi)polaron absorption at each dopant/polymer ratio (Figure S7 in the SI), suggesting that the PzDPP polymer can be more efficiently doped than the TDPP polymer. In *o*-dichlorobenzene (*o*-DCB) solution, P(PzDPP-CT2) also shows stronger polaron absorption than P(TDPP-CT2) after doping (Figure S6 in the SI), indicating the PzDPP polymer is more easily doped in solution state.

The ultraviolet photoelectron spectroscopy (UPS) and X-ray photoelectron spectroscopy (XPS) measurements also support the absorption spectra results. The secondary electron cutoff of P(PzDPP-CT2) shifts by 0.75 eV when doped with 60% *N*-DMBI, equivalent to an upward movement of its Fermi level by 0.75 eV, much larger than the shift of P(TDPP-CT2) (0.06 eV) under the same dopant/polymer ratio (Figure 2d). The XPS data of the doped polymers also clearly demonstrate that

DOI: 10.1021/jacs.9b10107
J. Am. Chem. Soc. 2019, 141, 20215−20221

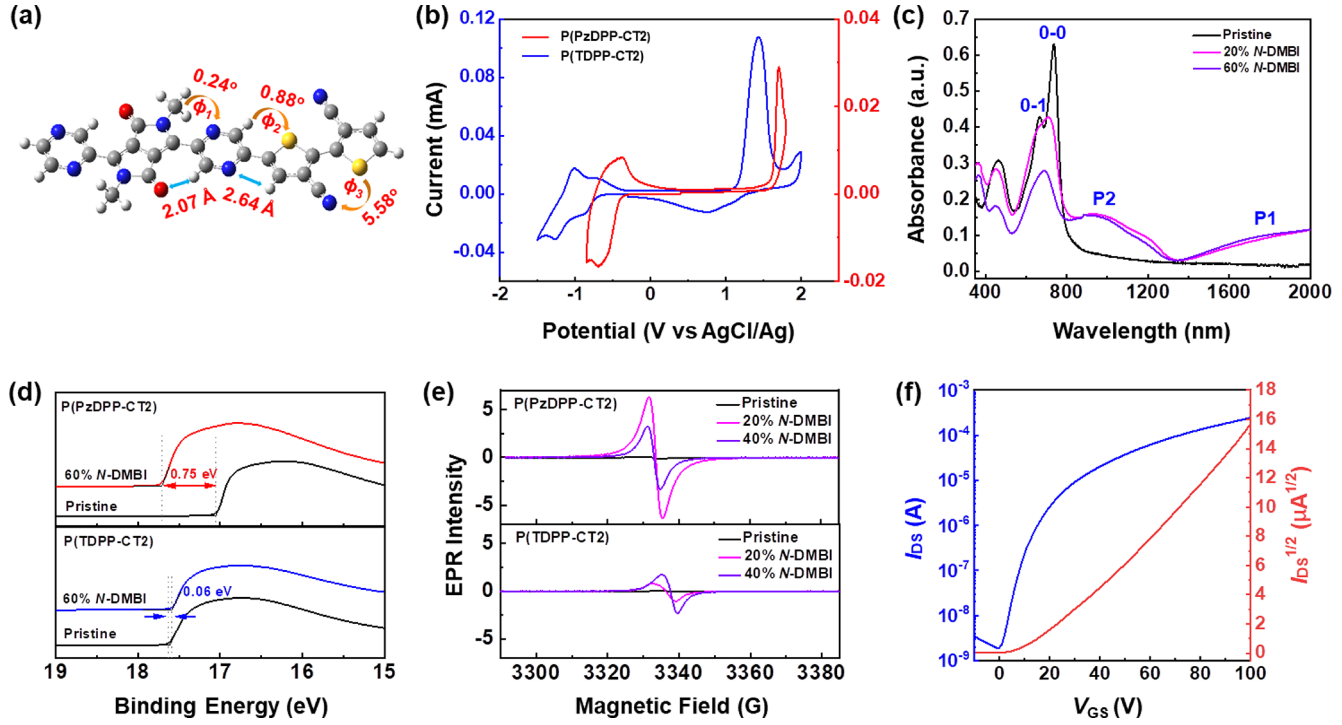

Figure 2. (a) DFT-optimized molecular model of the P(PzDPP-CT2) fragment (B3LYP/6-311G(d,p)). Long alkyl chains were replaced with methyl groups to simplify the calculation. (b) Cyclic voltammograms of both polymers in a thin film. (c) UV−vis−NIR absorption spectra of pristine and *N*-DMBI-doped P(PzDPP-CT2) in thin film. (d) UPS binding energy of the pristine and the doped P(PzDPP-CT2) (top) and P(TDPP-CT2) (bottom) films. (e) EPR signals of the pristine and the doped P(PzDPP-CT2) (top) and P(TDPP-CT2) (bottom) at different dopant/polymer weight ratios. (f) Transfer characteristics for the pristine polymer P(PzDPP-CT2) (W = 100 μm, L = 5 μm, C_i = 3.7 nF cm^{-2}).

P(PzDPP-CT2) is more readily n-doped with *N*-DMBI than P(TDPP-CT2). As the doping reaction is accompanied by the generation of *N*-DMBI$^+$ (402 eV), the doping level of the films could be estimated by the analysis of the *N*-DMBI$^+$ peak. At each doping concentration, the peak ratio between *N*-DMBI$^+$ and other N (1s) peaks in P(PzDPP-CT2) film is larger than that of the doped P(TDPP-CT2) film (Figure S10 in the SI).

The electron paramagnetic resonance (EPR) spectroscopy was used to evaluate the numbers of radicals formed in the polymer after doping. In the EPR spectroscopy, no observable radical signal was observed in both pristine polymers. After doped with 20% *N*-DMBI, P(PzDPP-CT2) showed a stronger radical signal than P(TDPP-CT2). The calculated spin density of the doped P(PzDPP-CT2) is approximately 1.61 × 10^{20} cm^{-3}, which is about 5 times that of the doped P(TDPP-CT2) (3.12 × 10^{19} cm^{-3}) (Figure 2e). When the *N*-DMBI fraction increased to 40%, the spin density of the doped P(TDPP-CT2) continuously increased to 5.36 × 10^{19} cm^{-3}; however, the spin density of the doped P(PzDPP-CT2) decreased to 1.15 × 10^{20} cm^{-3}. This result indicates that bipolarons or other species without radical signals were formed in P(PzDPP-CT2) at higher doping levels.[33,34]

Thermoelectric and Charge Transport Measurement. The thermoelectric properties of the doped P(PzDPP-CT2) and P(TDPP-CT2) films were studied in a vacuum chamber to avoid temperature fluctuation and O_2/water dedoping. To accurately evaluate the thermoelectric performance of both polymers, all devices were fabricated and patterned according to the criteria proposed by Reenen and Kemerink.[35] The films were encapsulated in case they were exposed to oxygen and water when they were transferred to the thermoelectric testing instrument. The conductivity decreased after patterning and transfer (as shown by the dashed line to the solid line in Figure 3). P(PzDPP-CT2) showed a maximal conductivity of 8.4 S cm^{-1} after doping with 40% *N*-DMBI. When the dopant ratio increased from 5% to 70%, the Seebeck coefficients of both polymers decreased because of the negative correlation between the Seebeck coefficient and charge carrier concentration[36] (Figure S19 in the SI). The Seebeck coefficient of P(TDPP-CT2) is higher than that of P(PzDPP-CT2), which is due to the higher charge carrier concentration in the P(PzDPP-CT2) film at each dopant/polymer ratio. To exclude the possible contribution of the ionic Seebeck coefficient, we carried out the test of the long-time thermovoltage of doped films, and the thermovoltage remained stable at a steady temperature difference for several cycles. So the contribution of the ionic Seebeck effect and short-term contributions can be excluded (Figures S17, S19 in the SI). Power factors (PFs) are calculated using the conductivities (solid lines) and the Seebeck coefficients measured at the same time and under the same condition (after transferring to the vacuum chamber). A maximal power factor of P(PzDPP-CT2) was obtained by varying the dopant fractions, yielding a high value of 57.3 μW m^{-1} K^{-2}. To the best of our knowledge, this value is the highest in solution-processable n-doped conjugated polymers. In contrast, the maximal electrical conductivity of the *N*-DMBI-doped P(TDPP-CT2) is only 0.39 S cm^{-1}, far below that of P(PzDPP-CT2), thus resulting in a lower maximal power factor of 9.3 μW m^{-1} K^{-2}. The conductivities of both polymers decrease at high doping concentrations (>40% or 30%), which was also observed in other *N*-DMBI-doped polymer systems.[7,9] This phenomenon is probably due to the damaging of the charge transport networks after introducing a large number of dopants.[14,17]

DOI: 10.1021/jacs.9b10107
J. Am. Chem. Soc. 2019, 141, 20215−20221

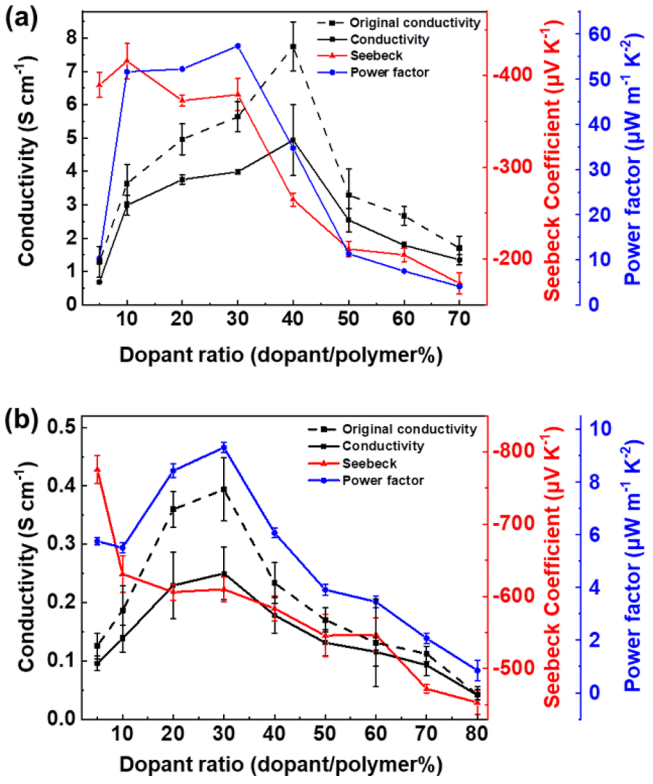

Figure 3. Electrical conductivities, Seebeck coefficients, and power factors of (a) P(PzDPP-CT2) and (b) P(TDPP-CT2) at different dopant/polymer ratios. The dashed lines show the original conductivities measured in a nitrogen glovebox. The solid lines are the thermoelectric parameters measured under a vacuum chamber.

The temperature-dependent electrical conductivity of the doped P(PzDPP-CT2) exhibits weaker temperature dependence compared with that of P(TDPP-CT2), suggesting the lower hopping barrier in the doped P(PzDPP-CT2) film (Figure S11 in the SI). The field-effect mobilities of the pristine P(PzDPP-CT2) and P(TDPP-CT2) were measured to understand their charge transport properties. The electron mobility of P(PzDPP-CT2) was evaluated to be 0.68 ± 0.11 cm^2 V^{-1} s^{-1} with a near-ideal n-type transport curve and a high on/off ratio (Figure 2f). After changing the solvent to 1-chloronaphthalene and optimizing the device fabrication conditions, the electron mobility of P(PzDPP-CT2) can be further increased to 1.67 cm^2 V^{-1} s^{-1} (Figure S13), which is comparable to other DPP-based unipolar n-type polymers.[9,37] In contrast, P(TDPP-CT2) showed ambipolar transport behavior with an electron mobility of 0.27 ± 0.05 cm^2 V^{-1} s^{-1} (Figure S12 in the SI). Note that compared with other DPP derivatives, such as thiophene-, pyridine-, and quinoline-flanked DPP, that typically show ambipolar transport behaviors,[22,38] our PzDPP polymer only shows n-type charge transport behavior with negligible hole injection. This again demonstrates that PzDPP is currently the most electron-deficient DPP building block and also suggests the promising application of PzDPP as the unipolar n-type polymer FET building block. Overall, we can conclude that, compared with the TDPP polymer, both the higher electron mobility and the higher doping level contribute to the higher n-type electrical conductivity of the PzDPP polymer.

Molecular Packing and Film Morphology. Grazing-incidence wide-angle X-ray scattering (GIWAXS) shows that both P(PzDPP-CT2) and P(TDPP-CT2) films have relatively weak crystallinity in pristine and doped films (Figure 4a, Figure S15 in the SI). The lamellar packing and $\pi-\pi$ stacking distances were calculated to be 29.7 and 3.38 Å for P(PzDPP-CT2) and 28.6 and 3.53 Å for P(TDPP-CT2). The shorter $\pi-\pi$ stacking distance of P(PzDPP-CT2) might be due to its stronger interactions, which is coincident with the temperature-dependent absorption spectrum study. When *N*-DMBI concentration increases, the lamellar packing and $\pi-\pi$ stacking distances remain almost unchanged in both the in-plane and the out-of-plane GIWAXS diffractions of both polymers (Figure 4b and Figure S15). As we know, X-ray diffraction characterization is mainly sensitive to the changes of the crystalline region of a polymer film but can hardly detect the changes occurring in the amorphous region. Therefore, these results indicate that the introduction of dopants does not significantly alter the crystalline regions of both polymers. Note that the $\pi-\pi$ stacking distances of the pristine and the 60% *N*-DMBI-doped P(PzDPP-CT2) films are 3.38 and 3.43 Å, respectively. These values are all obviously smaller than those of the P(TDPP-CT2) (3.53 and 3.51 Å, respectively), suggesting that closer $\pi-\pi$ stacking distance and stronger interchain interactions in the PzDPP polymer do not impede the efficient n-doping.

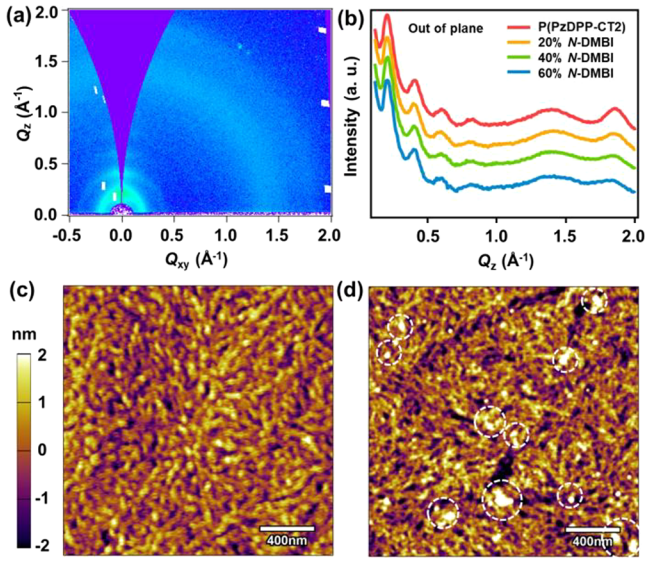

Figure 4. (a) 2D GIWAXS patterns of the 60% *N*-DMBI-doped P(PzDPP-CT2). (b) Out-of-plane GIWAXS plots of P(PzDPP-CT2) in pristine and doped conditions. AFM height images of (c) the pristine (RMS = 0.83 nm) and (d) the 60% *N*-DMBI-doped P(PzDPP-CT2) film (RMS = 0.92 nm). The circles show the large aggregates observed in the polymer film.

Atomic force microscopy (AFM) height images show that pristine P(PzDPP-CT2) and P(TDPP-CT2) films have a very smooth surface with a root-mean-square surface roughness of 0.83 and 0.63 nm. After doping, both polymers exhibit good miscibility. Only some large aggregates are observed at high doping concentrations (Figure 4d). Since the crystalline regions of both polymers do not show significant changes in GIWAXS, we tentatively propose that the dopants may exist in the amorphous regions of the polymer films. The large aggregates observed in AFM at high dopant concentrations may cause the charge carrier scattering and large grain

DOI: 10.1021/jacs.9b10107
J. Am. Chem. Soc. 2019, 141, 20215−20221

boundaries,[39] leading to decreased conductivity at higher dopant/polymer ratios.

To further understand the charge transport mechanism after doping, we measured the mobilities of P(PzDPP-CT2) films doped with 1% and 2% *N*-DMBI. The mobility increases as the *N*-DMBI concentration increases (Figure S18). In the pristine film, the electron mobility is determined to be 0.63 ± 0.23 $cm^2 V^{-1} s^{-1}$. After doping, the mobility of the polymer film increased to 0.91 ± 0.15 $cm^2 V^{-1} s^{-1}$ for 1% doping and to 1.20 ± 0.33 $cm^2 V^{-1} s^{-1}$ for 2% doping. These results suggest that electron mobilities could be further improved after being lightly n-doped, which is probably due to the reduced charge-trapping effects after doping.[40] Under heavy doping (2% to 40%), if the crystalline regions of the polymer film were not significantly damaged due to the above-mentioned "amorphous region doping", high electron mobility and high charge carrier concentration could be simultaneously realized, thereby leading to high electrical conductivity. In addition, a recent study suggests that the good miscibility between polymer and dopant and less energetic disorder in the polymer film can lead to a higher Seebeck coefficient and PF,[41] which might help to explain the high PF in our polymer/dopant system.

Previous strategies using either nonplanar donor units[11] or ethylene glycol side chains[10] to enhance the n-doping efficiency in n-type conjugated polymers always result in weaker interchain interactions or lower electron mobilities and finally low conductivities. In this work, our PzDPP polymer realizes closer $\pi-\pi$ stacking, higher electron mobility, and higher electrical conductivity at the same time, suggesting that without obviously sacrificing polymer interchain interactions, efficient n-doping and high thermoelectric performance can be achieved in PzDPP polymers.

In conclusion, we have designed and synthesized a new DPP derivative, PzDPP, that has the deepest LUMO level in all reported DPP building blocks for conjugated polymers. With the new building block and careful polymer engineering, P(PzDPP-CT2) has shown high electrical conductivities of up to 8.4 S cm^{-1}, much higher than the reference TDPP polymer and other n-doped D−A type polymers. Due to the much-improved conductivity, a high power factor of 57.3 $\mu W m^{-1} K^{-2}$ is also obtained, which is a new record in solution-processable n-doped conjugated polymers (Table S3 in the SI).[42] These results demonstrate that PzDPP is a promising high-performance building block for n-type organic thermoelectrics.

■ ASSOCIATED CONTENT

Supporting Information

The Supporting Information is available free of charge at https://pubs.acs.org/doi/10.1021/jacs.9b10107.

Device fabrication details; GPC, TGA, and DSC traces; UV−vis−NIR spectra; XPS data; additional GIWAXS and AFM images; monomer and polymer synthesis and characterization (PDF)

■ AUTHOR INFORMATION

Corresponding Author

*tinglei@pku.edu.cn

ORCID

Ze-Fan Yao: 0000-0001-5590-0768

Jie-Yu Wang: 0000-0002-1903-8928

Xiaodan Gu: 0000-0002-1123-3673

Ting Lei: 0000-0001-8190-9483

Author Contributions

#X. Yan and M. Xiong contributed equally to this work.

Notes

The authors declare no competing financial interest.

■ ACKNOWLEDGMENTS

This work is supported by the Key-Area Research and Development Program of Guangdong Province (2019B010934001) and the Beijing Natural Science Foundation (2192020). The scattering component in this article is supported by U.S. Department of Energy, Office of Science, Office of Basic Energy Science, under award number DE-SC0019361. The authors thank beamline BL14B1 (Shanghai Synchrotron Radiation Facility) for providing beam time.

■ REFERENCES

(1) Berggren, M.; Nilsson, D.; Robinson, N. D. Organic Materials for Printed Electronics. *Nat. Mater.* **2007**, *6*, 3−5.

(2) Molina-Lopez, F.; Gao, T. Z.; Kraft, U.; Zhu, C.; Öhlund, T.; Pfattner, R.; Feig, V. R.; Kim, Y.; Wang, S.; Yun, Y.; Bao, Z. Inkjet-Printed Stretchable and Low Voltage Synaptic Transistor Array. *Nat. Commun.* **2019**, *10*, 2676.

(3) Jia, H.; Lei, T. Emerging Research Directions for n-Type Conjugated Polymers. *J. Mater. Chem. C* **2019**, *7*, 12809−12821.

(4) Hong, S.; Gu, Y.; Seo, J. K.; Wang, J.; Liu, P.; Meng, Y. S.; Xu, S.; Chen, R. Wearable Thermoelectrics for Personalized Thermoregulation. *Sci. Adv.* **2019**, *5*, No. eaaw0536.

(5) Kim, G.-H.; Shao, L.; Zhang, K.; Pipe, K. P. Engineered Doping of Organic Semiconductors for Enhanced Thermoelectric Efficiency. *Nat. Mater.* **2013**, *12*, 719−723.

(6) Xia, Y.; Sun, K.; Ouyang, J. Solution-Processed Metallic Conducting Polymer Films as Transparent Electrode of Optoelectronic Devices. *Adv. Mater.* **2012**, *24*, 2436−2440.

(7) Lu, Y.; Yu, Z.-D.; Zhang, R.-Z.; Yao, Z.-F.; You, H.-Y.; Jiang, L.; Un, H.-I.; Dong, B.-W.; Xiong, M.; Wang, J.-Y.; Pei, J. Rigid Coplanar Polymers for Stable n-Type Polymer Thermoelectrics. *Angew. Chem., Int. Ed.* **2019**, *58*, 11390−11394.

(8) Wang, S.; Sun, H.; Erdmann, T.; Wang, G.; Fazzi, D.; Lappan, U.; Puttisong, Y.; Chen, Z.; Berggren, M.; Crispin, X.; Kiriy, A.; Voit, B.; Marks, T. J.; Fabiano, S.; Facchetti, A. A Chemically Doped Naphthalenediimide-Bithiazole Polymer for n-Type Organic Thermoelectrics. *Adv. Mater.* **2018**, *30*, 1801898.

(9) Yang, C.-Y.; Jin, W.-L.; Wang, J.; Ding, Y.F.; Nong, S.; Shi, K.; Lu, Y.; Dai, Y.-Z.; Zhuang, F.-D.; Lei, T.; Di, C.-A.; Zhu, D.; Wang, J.-Y.; Pei, J. Enhancing the n-Type Conductivity and Thermoelectric Performance of Donor−Acceptor Copolymers through Donor Engineering. *Adv. Mater.* **2018**, *30*, 1802850.

(10) Liu, J.; Ye, G.; van der Zee, B.; Dong, J.; Qiu, X. ; Liu, Y. ; Portale, G.; Chiechi, R. C.; Koster, L. J. A. N-Type Organic Thermoelectrics of Donor-Acceptor Copolymers: Improved Power Factor by Molecular Tailoring of the Density of States. *Adv. Mater.* **2018**, *30*, 1804290.

(11) Perry, E. E.; Chiu, C.-Y.; Moudgil, K.; Schlitz, R. A.; Takacs, C. J.; O'Hara, K. A.; Labram, J. G.; Glaudell, A. M.; Sherman, J. B.; Barlow, S.; Hawker, C. J.; Marder, S. R.; Chabinyc, M. L. High Conductivity in a Nonplanar n-Doped Ambipolar Semiconducting Polymer. *Chem. Mater.* **2017**, *29*, 9742−9750.

(12) Zhao, X.; Madan, D.; Cheng, Y.; Zhou, J.; Li, H.; Thon, S. M.; Bragg, A. E.; DeCoster, M. E.; Hopkins, P. E.; Katz, H. E. High Conductivity and Electron-Transfer Validation in an n-Type Fluoride-Anion-Doped Polymer for Thermoelectrics in Air. *Adv. Mater.* **2017**, *29*, 1606928.

(13) Wang, S.; Sun, H.; Ail, U.; Vagin, M.; Persson, P. O. A.; Andreasen, J. W.; Thiel, W.; Berggren, M.; Crispin, X.; Fazzi, D.; Fabiano, S. Thermoelectric Properties of Solution-Processed n-Doped

DOI: 10.1021/jacs.9b10107
J. Am. Chem. Soc. 2019, 141, 20215−20221

Ladder-Type Conducting Polymers. *Adv. Mater.* **2016**, *28*, 10764−10771.
(14) Shi, K.; Zhang, F.; Di, C.-A.; Yan, T.-W.; Zou, Y.; Zhou, X.; Zhu, D.; Wang, J.-Y.; Pei, J. Toward High Performance n-Type Thermoelectric Materials by Rational Modification of BDPPV Backbones. *J. Am. Chem. Soc.* **2015**, *137*, 6979−6982.
(15) Liu, J.; Qiu, L.; Alessandri, R.; Qiu, X.; Portale, G.; Dong, J.; Talsma, W.; Ye, G.; Sengrian, A. A.; Souza, P. C. T.; Loi, M. A.; Chiechi, R. C.; Marrink, S. J.; Hummelen, J. C.; Koster, L. J. A. Enhancing Molecular n-Type Doping of Donor−Acceptor Copolymers by Tailoring Side Chains. *Adv. Mater.* **2018**, *30*, 1704630.
(16) Liu, J.; Shi, Y.; Dong, J.; Nugraha, M. I.; Qiu, X.; Su, M.; Chiechi, R. C.; Baran, D.; Portale, G.; Guo, X.; Koster, L. J. A. Overcoming Coulomb Interaction Improves Free-Charge Generation and Thermoelectric Properties for n-Doped Conjugated Polymers. *ACS Energy Lett.* **2019**, *4*, 1556−1564.
(17) Kiefer, D.; Giovannitti, A.; Sun, H.; Biskup, T.; Hofmann, A.; Koopmans, M.; Cendra, C.; Weber, S.; Koster, L. J. A.; Olsson, E.; Rivnay, J.; Fabiano, S.; McCulloch, I.; Müller, C. Enhanced n-Doping Efficiency of a Naphthalenediimide-Based Copolymer through Polar Side Chains for Organic Thermoelectrics. *ACS Energy Lett.* **2018**, *3*, 278−285.
(18) Mei, J.; Diao, Y.; Appleton, A. L.; Fang, L.; Bao, Z. Integrated Materials Design of Organic Semiconductors for Field-Effect Transistors. *J. Am. Chem. Soc.* **2013**, *135*, 6724−6746.
(19) Lei, T.; Wang, J.-Y.; Pei, J. Design, Synthesis, and Structure-Property Relationships of Isoindigo-Based Conjugated Polymers. *Acc. Chem. Res.* **2014**, *47*, 1117−1126.
(20) Yang, J.; Zhao, Z.; Wang, S.; Guo, Y.; Liu, Y. Insight into High-Performance Conjugated Polymers for Organic Field-Effect Transistors. *Chem.* **2018**, *4*, 2748−2785.
(21) Gao, Y.; Deng, Y.; Tian, H.; Zhang, J.; Yan, D.; Geng, Y.; Wang, F. Multifluorination toward High-Mobility Ambipolar and Unipolar n-Type Donor−Acceptor Conjugated Polymers Based on Isoindigo. *Adv. Mater.* **2017**, *29*, 1606217.
(22) Sun, B.; Hong, W.; Yan, Z.; Aziz, H.; Li, Y. Record High Electron Mobility of 6.3 cm^2 $V^{-1}s^{-1}$ Achieved for Polymer Semiconductors Using a New Building Block. *Adv. Mater.* **2014**, *26*, 2636−2642.
(23) Tsao, H. N.; Cho, D. M.; Park, I.; Hansen, M. R.; Mavrinskiy, A.; Yoon, D. Y.; Graf, R.; Pisula, W.; Spiess, H. W.; Müllen, K. Ultrahigh Mobility in Polymer Field-Effect Transistors by Design. *J. Am. Chem. Soc.* **2011**, *133*, 2605−2612.
(24) Kang, I.; Yun, H.-J.; Chung, D. S.; Kwon, S.-K.; Kim, Y.-H. Record High Hole Mobility in Polymer Semiconductors via Side-Chain Engineering. *J. Am. Chem. Soc.* **2013**, *135*, 14896−14899.
(25) Kang, K.; Watanabe, S.; Broch, K.; Sepe, A.; Brown, A.; Nasrallah, I.; Nikolka, M.; Fei, Z.; Heeney, M.; Matsumoto, D.; Marumoto, K.; Tanaka, H.; Kuroda, S.; Sirringhaus, H. 2D Coherent Charge Transport in Highly Ordered Conducting Polymers Doped by Solid State Diffusion. *Nat. Mater.* **2016**, *15*, 896−902.
(26) Mauck, C. M.; Hartnett, P. E.; Margulies, E. A.; Ma, L.; Miller, C. E.; Schatz, G. C.; Marks, T. J.; Wasielewski, M. R. Singlet Fission via an Excimer-Like Intermediate in 3,6-Bis(thiophen-2-yl)-diketopyrrolopyrrole Derivatives. *J. Am. Chem. Soc.* **2016**, *138*, 11749−11761.
(27) Wang, Y.; Hasegawa, T.; Matsumoto, H.; Mori, T.; Michinobu, T. High-Performance n-Channel Organic Transistors Using High-Molecular-Weight Electron-Defcient Copolymers and Amine-Tailed Self-Assembled Monolayers. *Adv. Mater.* **2018**, *30*, 1707164.
(28) Naab, B. D.; Guo, S.; Olthof, S.; Evans, E. G. B.; Wei, P.; Millhauser, G. L.; Kahn, A.; Barlow, S.; Marder, S. R.; Bao, Z. Mechanistic Study on the Solution-Phase n-Doping of 1,3-Dimethyl-2-aryl-2,3-dihydro-1H-benzoimidazole Derivatives. *J. Am. Chem. Soc.* **2013**, *135*, 15018−15025.
(29) Schlitz, R. A.; Brunetti, F. G.; Glaudell, A. M.; Miller, P. L.; Brady, M. A.; Takacs, C. J.; Hawker, C. J.; Chabinyc, M. L. Solubility-Limited Extrinsic n-Type Doping of a High Electron Mobility Polymer for Thermoelectric Applications. *Adv. Mater.* **2014**, *26*, 2825−2830.
(30) Wei, P.; Oh, J. H.; Dong, G.; Bao, Z. Use of a 1H-Benzoimidazole Derivative as an n-Type Dopant and To Enable Air-Stable Solution-Processed n-Channel Organic Thin-Film Transistors. *J. Am. Chem. Soc.* **2010**, *132*, 8852−8853.
(31) Naab, B. D.; Gu, X.; Kurosawa, T.; To, J. W. F.; Salleo, A.; Bao, Z. Role of Polymer Structure on the Conductivity of N-Doped Polymers. *Adv. Electron. Mater.* **2016**, *2*, 1600004.
(32) Brédas, J. L.; Street, G. B. Polarons, Bipolarons, and Solitons in Conducting Polymers. *Acc. Chem. Res.* **1985**, *18*, 309−315.
(33) Domagala, W.; Pilawa, B.; Lapkowski, M. Quantitative in-Situ EPR Spectroelectrochemical Studies of Doping Processes in Poly(3,4-alkylenedioxythiophene)s Part 1: PEDOT. *Electrochim. Acta* **2008**, *53*, 4580−4590.
(34) Bubnova, O.; Khan, Z. U.; Wang, H.; Braun, S.; Evans, D. R.; Fabretto, M.; Hojati-Talemi, P.; Dagnelund, D.; Arlin, J.-B.; Geerts, Y. H.; Desbief, S.; Breiby, D. W.; Andreasen, J. W.; Lazzaroni, R.; Chen, W. M.; Zozoulenko, I.; Fahlman, M.; Murphy, P. J.; Berggren, M.; Crispin, X. Semi-Metallic Polymers. *Nat. Mater.* **2014**, *13*, 190−194.
(35) Reenen, S. V.; Kemerink, M. Correcting for Contact Geometry in Seebeck Coefficient Measurements of Thin Film Devices. *Org. Electron.* **2014**, *15*, 2250−2255.
(36) Snyder, G. J.; Toberer, E. S. Complex Thermoelectric Materials. *Nat. Mater.* **2008**, *7*, 105−114.
(37) Kim, H. S.; Huseynova, G.; Noh, Y.-Y.; Hwang, D.-H. Modulation of Majority Charge Carrier from Hole to Electron by Incorporation of Cyano Groups in Diketopyrrolopyrrole-Based Polymers. *Macromolecules* **2017**, *50*, 7550−7558.
(38) Ni, Z.; Dong, H.; Wang, H.; Ding, S.; Zou, Y.; Zhao, Q.; Zhen, Y.; Liu, F.; Jiang, L.; Hu, W. Quinoline-Flanked Diketopyrrolopyrrole Copolymers Breaking through Electron Mobility over 6 cm^2 V^{-1} s^{-1} in Flexible Thin Film Devices. *Adv. Mater.* **2018**, *30*, 1704843.
(39) Un, H.-I.; Gregory, S. A.; Mohapatra, S. K.; Xiong, M.; Longhi, E.; Lu, Y.; Rigin, S.; Jhulki, S.; Yang, C.-Y.; Timofeeva, T. V.; Wang, J.-Y.; Yee, S. K.; Barlow, S.; Marder, S. R.; Pei, J. Understanding the Effects of Molecular Dopant on n-Type Organic Thermoelectric Properties. *Adv. Energy Mater.* **2019**, *9*, 1900817.
(40) Olthof, S.; Mehraeen, S.; Mohapatra, S. K.; Barlow, S.; Coropceanu, V.; Brédas, J.-L.; Marder, S. R.; Kahn, A. Ultralow Doping in Organic Semiconductors: Evidence of Trap Filling. *Phys. Rev. Lett.* **2012**, *109*, 176601.
(41) Boyle, C. J.; Upadhyaya, M.; Wang, P.; Renna, L. A.; Lu-Díaz, M.; Jeong, S. P.; Hight-Huf, N.; Korugic-Karasz, L.; Barnes, M. D.; Aksamija, Z.; Venkataraman, D. Tuning Charge Transport Dynamics via Clustering of Doping in Organic Semiconductor Thin Films. *Nat. Commun.* **2019**, *10*, 2827.
(42) Russ, B.; Glaudell, A.; Urban, J. J.; Chabinyc, M. L.; Segalman, R. A. Organic Thermoelectric Materials for Energy Harvesting and Temperature Control. *Nat. Rev. Mater.* **2016**, *1*, 16050.

DOI: 10.1021/jacs.9b10107
J. Am. Chem. Soc. 2019, 141, 20215−20221